# Solution Structure of μ-Conotoxin PIIIA, a Preferential Inhibitor of Persistent Tetrodotoxin-sensitive Sodium Channels*

**Katherine J. Nielsen‡, Michael Watson§, David J. Adams§, Anna K. Hammarström¶, Peter W. Gage¶, Justine M. Hill‡, David J. Craik‡∥, Linda Thomas‡, Denise Adams‡, Paul F. Alewood‡, and Richard J. Lewis‡§\*\***

*From the ‡Institute for Molecular Bioscience, University of Queensland, Brisbane 4072, Australia, the §School of Biomedical Sciences, University of Queensland, Brisbane 4072, Australia, and the ¶Division of Biochemistry and Molecular Biology, John Curtin School of Medical Research, Australian National University, Canberra, Australian Capital Territory 2601, Australia*

μ-Conotoxins are peptide inhibitors of voltage-sensitive sodium channels (VSSCs). Synthetic forms of μ-conotoxins PIIIA and PIIIA-(2–22) were found to inhibit tetrodotoxin (TTX)-sensitive VSSC current but had little effect on TTX-resistant VSSC current in sensory ganglion neurons. In rat brain neurons, these peptides preferentially inhibited the persistent over the transient VSSC current. Radioligand binding assays revealed that PIIIA, PIIIA-(2–22), and μ-conotoxin GIIIB discriminated among TTX-sensitive VSSCs in rat brain, that these and GIIIC discriminated among the corresponding VSSCs in human brain, and GIIIA had low affinity for neuronal VSSCs. ¹H NMR studies found that PIIIA adopts two conformations in solution due to *cis/trans* isomerization at hydroxyproline 8. The major *trans* conformation results in a three-dimensional structure that is significantly different from the previously identified conformation of μ-conotoxins GIIIA and GIIIB that selectively target TTX-sensitive muscle VSSCs. Comparison of the structures and activity of PIIIA to muscle-selective μ-conotoxins provides an insight into the structural requirements for inhibition of different TTX-sensitive sodium channels by μ-conotoxins.

Voltage-sensitive sodium channels (VSSCs)[1] underlie the influx of sodium ions responsible for action potentials in excitable cells (1). Based on their susceptibility to block by tetrodotoxin (TTX), VSSCs can be divided into TTX-sensitive (TTX-S) and TTX-resistant (TTX-R) classes. Members of both classes share considerable sequence homology and are closely related structurally (2). These include the neuronal TTX-S type I/$Na_v1.1$, type II/$Na_v1.2$, type III/$Na_v1.3$, PN1/$Na_v1.7$ and PN4/$Na_v1.6$, and the skeletal muscle TTX-S μ1/$Na_v1.4$. The TTX-R sodium channels include the cardiac H1/$Na_v1.5$, which is partially TTX-resistant, and the neuronal TTX-R channels SNS/PN3/$Na_v1.8$ and NaN/PN5/$Na_v1.9$ (2). A number of these VSSC subtypes are implicated in clinical states such as pain (3–6), stroke (7, 8), and epilepsy (9, 10). Persistent (noninactivating) forms of the TTX-S sodium channel current that underlie repetitive firing (11, 12) have less well defined origins but may involve $Na_v1.3$ (13) or $Na_v1.6$ (11) and are enhanced by hypoxia (14–16) and nitric oxide (17). Most TTX-S sodium channels types have a heterogeneous distribution in human brain (18).

VSSCs are inhibited by local anesthetics and modulated by toxins that act at one inhibitory site (site 1) and at least four other sites that result in excitatory actions. μ-Conotoxins from the venom of marine cone snails act selectively to occlude the pore of the VSSC by competing with TTX and saxitoxin (STX) for binding to site 1 in the P-loop region of the α subunit. To date, sequences for four members of the three-loop μ-conotoxin class have been published (Table I). GIIIA–GIIIC from *Conus geographus* venom are potent blockers of skeletal muscle but not neuronal VSSCs. The three-dimensional structures of selected μ-conotoxins (19, 20) have been used to describe the architecture of the outer vestibule of the VSSC (21–25). The most recently described member of this class is μ-conotoxin PIIIA (26) from *C. purpurescens* (Fig. 1). PIIIA is notable for its ability to inhibit neuronal as well as muscle TTX-S sodium channels (26) and to discriminate among VSSCs in rat brain (27). Thus, PIIIA is the first peptide toxin for investigating the architecture of site 1 of neuronal VSSCs.

Previous studies on GIIIA (21, 22) have revealed that the cationic residues, particularly Arg[13], are important for the high potency of this peptide at $Na_v1.4$ (see Fig. 1). The high sequence identity and similarities in the three-dimensional structures of GIIIA and GIIIB (19, 20) provide a rational basis for comparison with PIIIA, which also contains a number of conserved residues and the same disulfide connectivities as GIIIA and GIIIB (and GIIIC). However, a number of primary structural differences are apparent between PIIIA and other μ-conotoxins, which may affect the relative position and orientation of backbone loops and their projecting side chains and thus allow PIIIA to interact with both neuronal and muscle forms of TTX-sensitive VSSCs.

To further investigate the potential of PIIIA as a probe of VSSCs, we determined its structure by ¹H NMR spectroscopy and characterized its mode of action on native tissues using electrophysiological and ligand binding approaches. These studies revealed that PIIIA and PIIIA-(2–22) preferentially inhibited the persistent TTX-S currents in rat hippocampal neurons, whereas in rat DRG the TTX-R current was spared. Comparisons of the three-dimensional structures of PIIIA, GIIIA, and GIIIB revealed important structural differences,

[1] The abbreviations used are: VSSC, voltage-sensitive sodium channel; TTX, tetrodotoxin; TTX-S, TTX-sensitive; TTX-R, TTX-resistant; TES, 2-{[2-hydroxy-1,1-bis(hydroxymethyl)ethyl]amino}ethanesulfonic acid; STX, saxitoxin; NOE, nuclear Overhauser effect; NOESY, NOE spectroscopy; Hyp, hydroxyproline; r.m.s., root mean square.
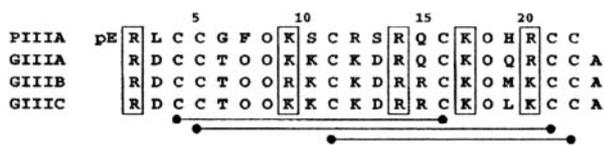
FIG. 1. **Primary sequence of μ-conotoxins GIIIA, GIIIB, GIIIC (60), and PIIIA (26) with disulfide connectivity indicated.** Standard one-letter codes are used for amino acids, except for pyroglutamic acid (*pE*) and hydroxyproline (*O*). Common residues found important for binding in GIIIA (21) are *boxed*. PIIIA-(2–22) is a truncated derivative of PIIIA in which the terminal pyroglutamate is absent. *Lines* indicate cysteine connectivity.

including an alternative major conformation accessed by PIIIA, which had not been identified previously in μ-conotoxins.

## EXPERIMENTAL PROCEDURES

### Peptide Synthesis

Peptides were prepared by Boc chemistry (28) using methods described for ω-conotoxins (29). The side chain protection chosen was Arg(tos), Asp(OcHex), Lys(CIZ), Ser(Bzl), and Cys(*p*-MeBzl). The crude reduced peptides were purified by preparative chromatography, using a 1% gradient (100% A to 80% B, 80 min) and UV detection at 230 nm. The reduced peptides were oxidized at a concentration of 0.02 mM in either aqueous 0.33 M NH$_4$OAc, 0.5 M guanidine HCl or aqueous 2 M NH$_4$OH. The solution was stirred for 3–5 days at pH 8.1. Purification of oxidized peptide was completed using preparative reversed phase high pressure liquid chromatography.

### Radioligand Binding

Whole rat brain (29), the human frontal cortex (30), and rat skeletal muscle (31) were homogenized in 50 mM HEPES (pH 7.4), filtered though 100-μm nylon mesh (muscle only), and centrifuged at 28,000 × *g* (10 min). The pellet was suspended in 50 mM HEPES, 10 mM EDTA (pH 7.4) for 30 min, centrifuged, and resuspended in 50 mM HEPES (pH 7.4). Radioligand binding studies were conducted in assay buffer (130 mM choline chloride, 5.4 mM KCl, 5.5 mM glucose, 0.8 mM MgSO$_4$, 1.8 mM CaCl$_2$, 50 mM HEPES (pH 7.4 with Tris base)). Assays were conducted on rat brain (18 μg of protein, 150-μl total volume), human brain (12 μg of protein, 150 μl), and rat muscle (50 μg of protein, 300 μl) that contained 5.6 nM [$^3$H]STX (14.9 Ci/mmol; Amersham Biosciences) and varying concentrations of μ-conotoxins in assay buffer. Assays were incubated for 1 h at 4 °C and filtered through GFB filters on a Tomtec harvester (brain) or a Millipore manifold (muscle) using wash buffer (163 mM choline chloride, 1.8 mM CaCl$_2$, 0.8 mM MgSO$_4$, 5.0 mM HEPES (pH 7.4 with Tris base)). Filters were dried, scintillant was added, and filters retained radioactivity measured on a Microbeta counter (Wallac).

### Electrophysiological Experiments

Electrophysiological experiments were conducted to further investigate the effect of PIIIA on TTX-S and TTX-R sodium channels in native tissue.

*Dissociation of Nodose and DRG Neurons*—Sensory neurons from rat nodose ganglia and dorsal root ganglia (DRG) were isolated as previously described (32, 33). Briefly, young rats (10–21 days) were killed by cervical dislocation, and the nodose and DRG were carefully removed. The ganglia were placed in physiological saline solution containing collagenase (~1.0 mg/ml type 2; Worthington-Biochemical) and incubated for 1 h at 37 °C in 95% air and 5% CO$_2$ for 24–48 h. Neurons from the nodose ganglia that were clear and round were selected for experiments. Small diameter cells (~20 μm) from the DRG were used, since these have previously been reported to predominantly express TTX-resistant Na$^+$ currents (34).

*Dissociation of Hippocampal CA1 Neurons*—Young rats (14–21 days) were anesthetized under CO$_2$ and decapitated with an animal guillotine. The brain was removed and transferred to ice-cold artificial cerebrospinal fluid (containing 124 mM NaCl, 26 mM NaH$_2$CO$_3$, 3 mM KCl, 1.3 mM MgSO$_4$, 2.5 mM NaH$_2$PO$_4$, and 20 mM glucose). The brain was mounted in a vibratome and bathed in ice-cold artificial cerebrospinal fluid equilibrated with 95% O$_2$ and 5% CO$_2$ while the 500-μm-thick slices were prepared. Brain slices were incubated for 30 min with 200 units/ml papain (Worthington), 1.1 mM cysteine (Sigma), 0.2 mM EDTA, 13.4 mM mercaptoethanol at 35 °C. Following incubation, the CA1 region was located, removed, and gently triturated using a fire-polished Pasteur pipette. Neurons of 10–15 μm were used, and cells that were flat, swollen, or grainy in appearance were avoided.

*Electrophysiological Recordings*—Whole cell Na$^+$ currents were recorded using the patch clamp technique. Patch pipettes (GC150F; Harvard Apparatus Ltd., Edenbridge, Kent, UK) were prepared that had resistances of between 1 and 2 megaohms (nodose and DRG neurons) and between 6 and 10 megaohms (CA1 neurons) when filled with pipette solution. Whole cell Na$^+$ currents from nodose and DRG neurons were made using a List EPC 7 amplifier (List Medical). Voltage steps were generated by a PC (Dell Pentium) running pClamp (Axon Instruments Inc., Union City, CA). Whole cell Na$^+$ currents from CA1 neurons were made using a Axopatch 1D amplifier (Axon Instruments) with voltage steps generated using a PC (Osborne 486-SX) running custom software (14, 15, 35).

*Solution and Toxins*—To record Na$^+$ currents from DRG and nodose neurons, patch pipettes were filled with the following solution: 135 mM CsF, 10 mM NaCl, 5 mM HEPES, with pH adjusted to 7.2 with CsOH. The bath solution contained 50 mM NaCl, 3 mM KCl, 90 mM tetraethylammonium chloride, 0.1 mM CdCl$_2$, 7.7 mM glucose, 10 mM HEPES, with pH adjusted to 7.4 with TEA-OH. To record Na$^+$ currents from CA1 neurons, the patch pipette solution contained the following solution: 125 mM CsF, 5 mM NaF, 10 mM KCl, 10 mM TES, with pH adjusted to 7.4 with KOH. The bath solution contained 135 mM NaCl, 5 mM KCl, 3 mM MgCl$_2$, 1 mM CaCl$_2$, 5 mM CoCl$_2$, 5 mM CsCl, 10 mM TES, with pH adjusted to 7.4 with NaOH.

*Data Analysis*—Three distinct Na$^+$ currents were measured: a transient TTX sensitive Na$^+$ current (TTX-S $I_{NaT}$), a transient TTX-resistant Na$^+$ current (TTX-R $I_{NaT}$), and a persistent TTX-sensitive Na$^+$ current (TTX-S $I_{NaP}$). The amplitude of evoked TTX-S $I_{NaT}$ was measured at its peak after subtraction of the current evoked in the presence of TTX (0.5–1 μM). The amplitude of the TTX-R $I_{NaT}$ was measured at least 2 min following the addition of 0.5–1 μM TTX. The amplitude of TTX-S $I_{NaP}$ was measured at the end of a 400-ms voltage step after subtraction of the current evoked in the presence of TTX (0.5–1 μM). All values are expressed as means ± S.E. with *n* indicating the number of cells in a given series of experiments. Comparisons of two means were made using Student's two-tailed unpaired *t* test.

### $^1$H NMR Spectroscopy

All NMR experiments were recorded on a Bruker ARX 500 spectrometer equipped with a *z*-gradient unit or on a Bruker DMX 750 spectrometer equipped with an *x,y,z*-gradient unit. Peptide concentrations were ~2 mM. PIIIA was examined in 95% H$_2$O, 5% D$_2$O (pH 3.0 and 5.5; 275–298 K) and in 50% aqueous CD$_3$CN (260–293 K). $^1$H NMR experiments recorded were NOESY (36, 37) with mixing times of 150, 200, and 400 ms, TOCSY (38) with a mixing time of 80 ms, DQF-COSY (39), and E-COSY in 100% D$_2$O (40). All spectra were run over 6024 Hz (500 MHz) or 8192 Hz (750 MHz) with 4 K data points, 400–512 free induction decays, 16–64 scans, and a recycle delay of 1 s. The solvent was suppressed using the WATERGATE sequence (41). Spectra were processed using UXNMR as described previously (29) and using Aurelia; subtraction of background was used to minimize T$_1$ noise. Chemical shift values were referenced internally to 4,4-dimethyl-4-silapentane-1-sulfonate at 0.00 ppm. Secondary Hα shifts were measured using random coil shift values of Wishart *et al.* (42). $^3J_{NH-Hα}$ coupling constants were measured as previously described (29).

### Distance Restraints and Structure Calculations

Peak volumes in NOESY spectra were classified as strong, medium, weak, and very weak, corresponding to upper bounds on interproton distance of 2.7, 3.5, 5.0, and 6.0 Å, respectively. Lower distance bounds were set to 1.8 Å. Appropriate pseudoatom corrections were made (43), and distances of 0.5 and 2.0 Å were added to the upper limits of restraints involving methyl and phenyl protons, respectively. $^3J_{NH-Hα}$ coupling constants were used to determine φ dihedral angle restraints (44), and in cases where $^3J_{NH-Hα}$ was 6–8 Hz and it was clear that a positive dihedral angle was not present, φ was restrained to −100 ± 70°. $^3J_{Hα-Hβ}$ coupling constants, together with relevant NOESY peak strengths, were used to determine x1 dihedral angle restraints (45). Where there was no diastereospecific assignment for a prochiral pair of protons, the largest upper bound for the two restraints was used. Where stereospecific assignments were established, these distances were specified explicitly.

Structures were calculated using the torsion angle dynamics/simulated annealing protocol in X-PLOR (46) version 3.8 using a modified geometric force field based on parhdg.pro. Structure refinements were performed using energy minimization (200 steps) under the influence of a full force field derived from Charmm (47) parameters. Structure modeling, visualization, and superimpositions were done using In-
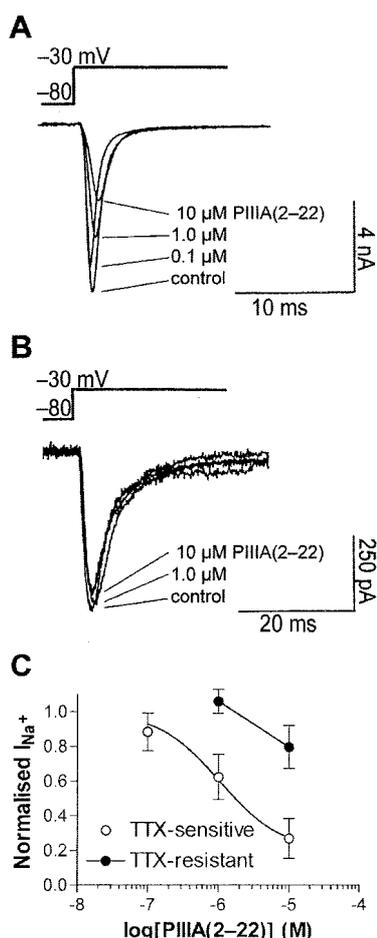
FIG. 3. **Effects of PIIIA-(2–22) on the transient and persistent TTX-sensitive Na$^+$ currents recorded from hippocampal CA1 neurons.** Na$^+$ currents recorded from a hippocampal CA1 neuron showing the effects of PIIIA-(2–22) on the transient TTX-sensitive Na$^+$ current and the persistent Na$^+$ current. *Inset*, the differential effects of PIIIA-(2–22) on the amplitude of the transient and persistent Na$^+$ current. Peak amplitudes of the transient and persistent current were normalized to the transient and persistent currents recorded in control solution. Each point represents the mean current amplitude from at least three cells obtained following a voltage step to −30 mV from a holding potential of −80 mV (prepulsed to −130 mV for 300 ms).



FIG. 2. **Effects of PIIIA-(2–22) on transient TTX-sensitive and TTX-resistant Na$^+$ currents recorded in nodose and DRG neurons.** Shown are Na$^+$ currents recorded from a nodose ganglia neuron (*A*) and a DRG neuron (*B*) in control solution and in the presence of 0.1–10 μM PIIIA-(2–22). The records shown in *B* were obtained in the continued presence of 1 μM TTX to measure effects on the TTX-R current. *C*, dose-response relationship showing the effects of PIIIA-(2–22) on the transient TTX-resistant Na$^+$ current recorded from DRG neurons (●) and the effects of PIIIA on the transient TTX-sensitive Na$^+$ current recorded from nodose neurons (○). Each point represents the mean current amplitude from at least three cells obtained following a voltage step to −30 mV from a holding potential of −80 mV.

sightII (MSI). Surface calculations, r.m.s. deviations, and hydrogen bond analysis were done using MOLMOL (48). The quality of the structures was analyzed using procheck-NMR (49).

### RESULTS

*Effects of PIIIA and PIIIA-(2–22) on Neuronal Whole Cell Na$^+$ Currents*—The effects of μ-conotoxin PIIIA and a truncated analogue, PIIIA-(2–22), were investigated on three distinct VSSCs found in neurons of the peripheral and central nervous system. Rat nodose ganglion neurons were used to investigate the transient TTX-sensitive voltage-dependent Na$^+$ current (TTX-S $I_{NaT}$), DRG neurons were used to investigate the transient TTX-resistant sodium current (TTX-R $I_{NaT}$) (34), and rat hippocampal neurons in the CA1 region were used to investigate the persistent TTX-sensitive sodium current (TTX-S $I_{NaP}$) (15, 50, 51).

PIIIA-(2–22) caused a concentration-dependent reduction in the peak amplitude of the TTX-S $I_{NaT}$ in rat nodose ganglia neurons (Fig. 2). In contrast, in rat DRG neurons (*n* = 12), PIIIA-(2–22) produced only a small reduction in the peak amplitude of the TTX-R $I_{NaT}$ (Fig. 2). High frequency stimulation can modify the degree of block by some neurotoxins that act in a use-dependent manner. Compared with control, 1 μM PIIIA-
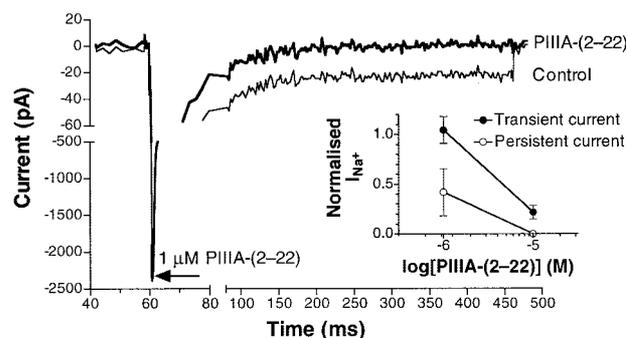
(2–22) failed to produce any use-dependent inhibition of peak TTX-S $I_{NaT}$ during 20 depolarizing pulses from a holding potential of −80 mV to a test potential of −30 mV for 25 ms delivered at a frequency of 20 Hz (*n* = 6). In rat hippocampal CA1 neurons, the addition of PIIIA-(2–22) to the bathing solution caused a concentration-dependent reduction in the peak amplitude of the TTX-S $I_{NaT}$ and the TTX-S $I_{NaP}$ (Fig. 3). Interestingly, PIIIA-(2–22) had a greater effect on the TTX-S $I_{NaP}$ than on the TTX-S $I_{NaT}$ (Fig. 3, *inset*). At 1 μM, the peak amplitude of the TTX-S $I_{NaT}$ was unaffected, whereas the amplitude of the TTX-S $I_{NaP}$ was reduced by ~70%.

The native μ-conotoxin, PIIIA, also reduced the TTX-S $I_{NaT}$ in rat nodose (*n* = 12), DRG (*n* = 3), and CA1 (*n* = 3) neurons (data not shown) with a similar potency to PIIIA-(2–22). PIIIA had a preferential effect on the persistent compared with the transient sodium current, being slightly more potent at reducing the amplitude of the TTX-S $I_{NaT}$ current in CA1 neurons than PIIIA-(2–22). In preliminary experiments, 10-min bath application of GIIIB (1–10 μM) had no effect on either the TTX-S or TTX-R $I_{NaT}$ in rat nodose or DRG neurons, respectively (*n* = 3; data not shown).

*Radioligand Binding Studies*—The ability of μ-conotoxins to displace [³H]STX from VSSCs in human and rat brain and rat skeletal muscle is shown in Fig. 4. All peptides were more potent at the rat skeletal muscle than rat brain VSSCs, with GIIIA and GIIIC showing most selectivity and PIIIA least selectivity. The pIC$_{50}$ values and percentage inhibition for these peptides are given in Table I. The data show that PIIIA and PIIIA-(2–22) have greatest potency at rat and human brain VSSCs, GIIIB has intermediate potency, and GIIIA and GIIIC have least potency. These peptides were less potent than TTX, with none able to fully displace [³H]STX from rat or human brain (relative to TTX displacement). PIIIA and PIIIA-(2–22) produced the largest displacement of [³H]STX, and GIIIA and GIIIC produced the least displacement. GIIIB was more effective at displacing [³H]STX from rat compared with human brain (Fig. 4, *A* and *B*). All displacement curves were best fitted with a Hill slope of −1.

*¹H NMR Spectroscopy*—PIIIA was examined by ¹H NMR spectroscopy in a range of different solvent conditions. In aqueous solution at pH 2.5–5.5 over 275–298 K, it was apparent that two conformations of PIIIA were present in a ~3:1 ratio. In aqueous solution at low pH over 283–298 K, the NH resonances of several residues, including 4–7, 10–12, 20, and 22,
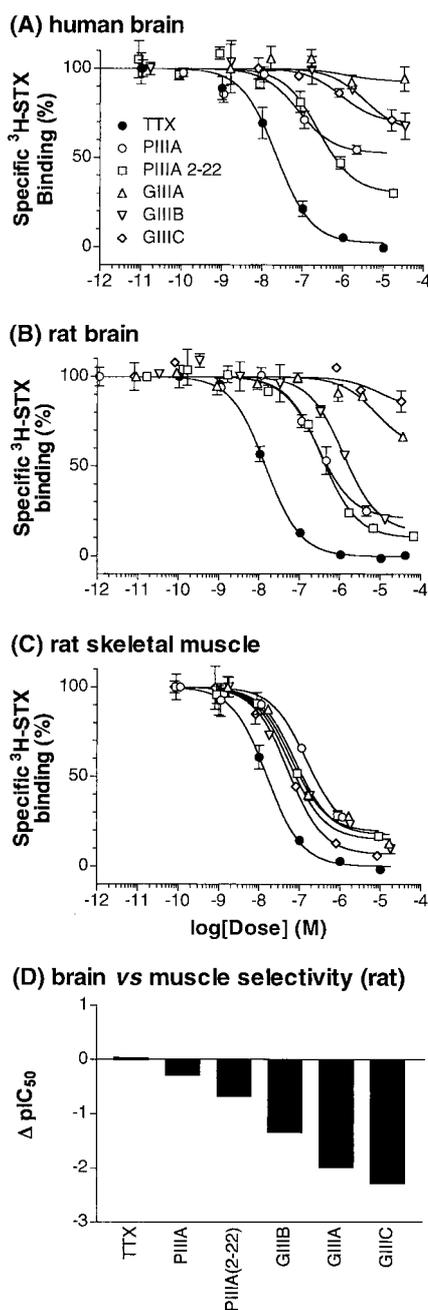
## (A) human brain



## (B) rat brain



## (C) rat skeletal muscle



## (D) brain vs muscle selectivity (rat)



Fig. 4. **Displacement of [³H]STX from brain and skeletal muscle VSSC by TTX and μ-conotoxins PIIIA, PIIIA-(2–22), GIIIA, GIIIB, and GIIIC.** *A*, human brain; *B*, rat brain; *C*, rat skeletal muscle; *D*, neuronal *versus* skeletal muscle selectivity in rat tissue. Legend refers to *A*, *B*, and *C*.

were broad, and that of Cys[21] was not observable. At higher pH values and lower temperatures (275 K), these peaks sharpened (residues 4 and 5) or separated into two distinct sets of peaks (residues 6 and 7, 10–12, 20, and 22) so that complete assignment of the major and a partial assignment of the minor conformations was possible. The assignment of PIIIA was improved by the addition of up to 50% CD$_3$CN, where the set of peaks arising from the minor conformation was less evident, and all resonances from the major conformation were present. Chemical shift assignments for PIIIA are given in Table II.

The two hydroxyproline (Hyp) residues in PIIIA are assigned as *trans* from the observation of strong Hδ-Hα$_{i-1}$ NOEs in the case of Hyp[8] and weak to medium Hδ-Hα$_{i-1}$, together with the stronger Hδ-Hα$_{i-1}$ NOEs in the case of Hyp[18] (52). The minor

conformation of PIIIA results from a *cis* conformation of Hyp[8], indicated by a Hδ-Hα$_{i-1}$ NOE to the preceding residue. PIIIA-(2–22) was also examined under similar conditions and found to have almost identical chemical shifts and to adopt two conformations in proportions similar to those observed for PIIIA. The remainder of this paper describes the major conformation observed for both PIIIA and PIIIA-(2–22), unless otherwise specified.

Secondary Hα shifts were used to examine the effects of solvent conditions on the backbone structure of PIIIA (Fig. 5). The shifts of PIIIA-(2–22) are also shown. These results clearly indicate that the backbone conformation is the same over a range of pH and solvent conditions for the native and truncated sequences. Similarly, the differences in Hβ shifts for AMX-bearing side chains, the Hδ shifts of the two Hyp residues, and the Hα shifts of Gly[6] remain largely unchanged over these conditions for PIIIA and PIIIA-(2–22) (data not shown), indicating that the conformations of the side chains are not significantly affected by changes in the solution environment. One exception is the Hβ protons of Cys[4], where the chemical shift differences between the Hβ2/Hβ3 protons increase with pH from 0.22 ppm at pH 3 to 0.66 ppm at pH 5. This is likely to arise from the ring current effect of an aromatic ring in proximity to the side chain of Cys[4] at higher pH.

Comparison of the Hα shifts of the minor conformation of PIIIA show significant differences from residues 7–11, indicating differences in backbone conformation in these regions. This is supported by differences in Hβ shifts that are evident from residues 6–11, and also at Cys[16]. Due to low signal intensities, it was not possible to observe peaks for both Hβ and protons of Cys[4], Cys[5], and Cys[21]. The ring current effects observed for Hβ protons of the major conformations of PIIIA were not present in the minor conformations, indicating a difference in the positions of either Phe[7] or His[19] relative to Cys[4].

Fig. 5 also compares the secondary Hα shifts of PIIIA with those of GIIIB, which adopts the same structure in solution as GIIIA (20). Overall, the trends are similar, indicating that the global fold of PIIIA and GIIIB are similar, as may be expected based on their identical disulfide pairings and loop sizes (Fig. 1). However, differences observed at residues 5–11 and 19–20 indicate that in some regions significant structural divergence exists. To directly address potential structural differences, we determined the three-dimensional structure of the major conformation PIIIA (see below). Interestingly, the secondary shifts of the minor conformation of PIIIA at residue 10 are more like those of GIIIB than the major form of PIIIA (Fig. 5), suggesting that the structure of the minor conformation of PIIIA is similar to the major conformation of GIIIB and GIIIA.

The local medium range NMR data that provide information on the secondary structure of PIIIA are given in Fig. 6. The presence of several Hα-NH$_{i+2}$, NH-NH$_{i+2}$, and Hα-NH$_{i+3}$ NOEs are indicative of the presence of several turns over the entire peptide and perhaps helix over residues 13–17. Although several long range NOEs are present, these did not correspond to the long range NOEs prescribing the β-hairpin of GIIIB (20). In fact, a number of long range NOEs were present that preclude a corresponding β-hairpin in the major conformation of PIIIA.

At higher pH values (>4.0 at 293 K) in aqueous solution or in 50% aqueous CD$_3$CN, the hydroxyl proton of Ser[13] side chain was observed. This resonance sharpened considerably with the lowering of temperature (275 K in H$_2$O; 260 K in CD$_3$CN) to reveal several medium range NOEs to residues 15 and 16, indicative of a hydrogen bond involving the side chain of Ser[13]. These flanking residues apparently stabilize the position of Arg[14], which has been shown to be crucial to the potency of

TABLE I

*Potency (pIC$_{50}$) and extent of inhibition (%) of [$^3$H]STX binding to VSSCs by μ-conotoxins and TTX*

95% confidence interval range for pIC$_{50}$ and percentage of inhibition are given in parenthesis.

| μ-Conotoxin | Human brain | Rat brain | Rat muscle |
|---|---|---|---|
| PIIIA | | | |
| Potency | 7.1 (7.6–6.6) | 6.5 (6.8–6.3) | 6.8 (7.1–6.5) |
| Inhibition | 47 (34–61)% | 79 (68–91)% | 81 (67–96)% |
| PIIIA-(2–22) | | | |
| Potency | 6.6 (7.0–6.2) | 6.4 (6.6–6.3) | 7.2 (7.4–7.0) |
| Inhibition | 70 (58–82)% | 90 (86–94)% | 81 (73–93)% |
| GIIIA | | | |
| Potency | Inactive | 5.1 (5.5–4.7) | 7.1 (7.3–6.9) |
| Inhibition | | 40 (28–52)% | 82 (76–89)% |
| GIIIB | | | |
| Potency | 5.5 (6.4–4.5) | 5.9 (6.2–5.7) | 7.2 (7.5–7.0) |
| Inhibition | 36 (17–54)% | 87 (72–101)% | 85 (78–92)% |
| GIIIC | | | |
| Potency | 6.0 (6.6–5.4) | Inactive | 7.3 (7.5–7.1) |
| Inhibition | 30 (20–41)% | | 93 (86–101)% |
| TTX | | | |
| Potency | 7.6 (7.8–7.4) | 7.8 (7.9–7.7) | 7.8 (7.9–7.7) |
| Inhibition | 98 (91–105)% | 100 (97–103)% | 100 (96–104)% |

TABLE II

*$^1$H chemical shifts of PIIIA*

Values not in parenthesis or brackets are for the major conformation in acetonitrile/H$_2$O (1:1) at pH 3.0 and 280 K; values in parentheses (major conformation) and brackets [minor conformation] were measured in H$_2$O at pH 5.0 and 285 K.

| Residue | NH | Hα | Hβ | Other |
|---|---|---|---|---|
| pGlu[1] | (7.98) | (4.29)[4.33] | | |
| Arg[2] | (8.53)[8.59] | 3.93 (4.25)[4.19] | 1.79 | Hγ 1.52; Hδ 2.92, 2.97; δNH 7.07 |
| Leu[3] | 8.47 (8.45)[8.48] | 4.40 (4.41)[4.32] | 1.57 | Hδ 0.88 |
| Cys[4] | 8.41 (8.43)[8.43] | 4.47 (4.58) | 2.34, 2.56 | |
| Cys[5] | 7.97 (8.03) | 4.14 (4.28) | 3.00, 3.47 | |
| Gly[6] | 8.38 (8.65)[7.84] | 3.83 (3.81, 3.82) [3.63, 4.11] | | |
| Phe[7] | 7.38 (7.43)[8.35] | 4.98 (5.05)[4.72] | 2.98, 3.13 | Hδ, Hε 7.19; Hζ 7.23 |
| Hyp[8] | | 4.41 (4.49)[4.28] | 2.05, 2.34 | Hγ 4.67; Hδ 3.75, 3.90 |
| Lys[9] | 8.55 (9.02)[8.87] | 3.98 (4.07)[4.11] | 1.93 | Hγ 1.34; Hδ 1.6; Hε 2.90; εNH$_3$ 7.49 |
| Ser[10] | 7.78 (7.92)[8.63] | 3.98 (4.05)[4.79] | 3.82, 3.37 | |
| Cys[11] | 8.08 (8.25)[8.34] | 4.39 (4.51)[4.62] | 3.12, 2.91 | |
| Arg[12] | 7.50 (7.52)[8.43] | 4.19 (4.28)[4.31] | 1.84, 1.98 | Hγ 1.66, 1.72; δNH 7.26 |
| Ser[13] | 7.73 (7.86)[7.90] | 4.48 (4.53)[4.43] | 3.99, 4.18 | (OH 5.72) |
| Arg[14] | 9.04 (9.19)[9.16] | 3.95 (4.01)[3.99] | 1.88 | Hγ1.67; Hδ 3.18; δNH 7.27 |
| Gln[15] | 8.51 (8.77)[8.72] | 4.10 (4.15)[4.16] | 2.01 | Hγ 2.39, 6.84; δNH$_2$ 7.46 |
| Cys[16] | 7.46 (7.62)[7.62] | 4.81 (4.81)[4.88] | 3.00, 3.18 | |
| Lys[17] | 8.06 (7.99)[8.06] | 4.21 (4.20)[4.16] | | Hγ 1.65, 1.70; Hδ 1.84 |
| Hyp[18] | | 4.58 (4.70) | 2.32, 1.79 | Hγ 4.46; Hδ 3.74, 3.24 |
| His[19] | 8.18 (8.17) | 4.37 (4.25)[4.24] | 3.31, 3.34 | Hε 7.35 |
| Arg[20] | 8.93 (9.22)[8.96] | 4.03 (4.12)[4.11] | 1.89 | Hγ 1.70; Hδ 3.17; δNH 7.24 |
| Cys[21] | 8.49 | 4.47 (4.48) | 3.11, 3.63 | |
| Cys[22] | 7.87 (8.13) | 4.86 (4.91)[4.89] | 3.11, 3.29 | NH$_2$ 7.30 |

PIIIA (26). No equivalent interaction has been observed previously for either GIIIA or GIIIB, although an Asp in the equivalent position could conceivably stabilize the crucial Arg[13] through the formation of a hydrogen bond with Gln[14] (GIIIA) or through a salt bridge with Arg[14] (GIIIB).

*Three-dimensional Structure of PIIIA*—A total of 372 NOE-derived distance restrained (149 intraresidual, 98 sequential, 125 long/medium range) and 27 dihedral (16 φ and 11 χ1) were used to generate a set of 50 structures of PIIIA. Of these, 46 converged to a similar fold with no NOE violations greater than 0.2 Å and no dihedral violations greater than 3°. The structural analysis and data indicating the quality of the structures are summarized in Table III. From this, it is apparent that the backbone structure is highly defined over residues 3–22, a conclusion that is supported by high average angular order parameters (S = 0.96) over this region for the φ and ψ backbone dihedral angles and low backbone r.m.s. deviations (Fig. 7A). Fig. 8A shows an overlay of the 20 lowest energy structures, which indicate that PIIIA is dominated by a series of turns over the N-terminal part of the molecule. From Ser[13] to the C terminus, the structure adopts a distorted helix, with devia-

tions from ideality at residues 18 and 19. Fig. 8B shows the positions of the side chains of residues 13−15, where it is clear that the exposure of Arg[14] is facilitated by the proximity of Ser[13] and Gln[15]. Analysis of the structures indicate the presence of hydrogen bonds between the side chain oxygen of Ser[13] and the backbone NH proton of Cys[15] (16 of 20 structures) or Gln[15] (11 of 20 structures) or the side chain amide protons of Gln[15] (1 of 20 structures), which would assist in stabilizing this configuration.

Examination of the structures of PIIIA reveals that the positions of some side chains are less precisely defined than others. Although there has been no quantitative investigation of the correlation between surface exposure and geometric precision within families of NMR-derived structures, it might be expected that more surface-exposed residues are less conformationally constrained than buried residues. To investigate this correlation for PIIIA, the surface area of each residue is compared with the heavy atom r.m.s. deviations for each residue in Fig. 7B. From this plot, it is evident that surface exposure correlates with r.m.s. deviation values ($r^2 = 0.83$ for all residues, $r^2 = 0.90$ for residues 3−22). This comparison pro-
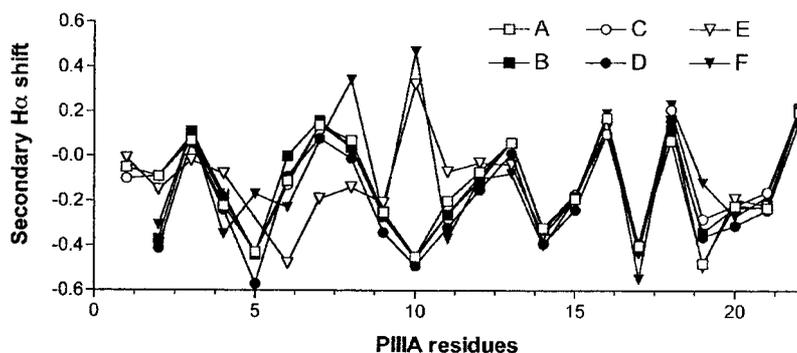
FIG. 5. **Secondary Hα shifts of PIIIA in aqueous solution at pH 4.5 (*A*), PIIIA-(2–22) in aqueous solution at pH 4.5 (*B*), PIIIA in aqueous solution at pH 3 (*C*), PIIIA-(2–22) in 50% aqueous CD$_3$CN at pH 3 (*D*), minor conformation of PIIIA in aqueous solution at pH 4.5 (*E*), and GIIIB in aqueous solution at pH 3.5 (20) (*F*).** The PIIIA and PIIIA-(2–22) measurements were made at 285 K. The numbering is based on PIIIA residues and alignment on the position of cysteine residues (see Fig. 1). The chemical shift for Cys$^5$ in the minor conformation of PIIIA is omitted, since it was not clearly observed.
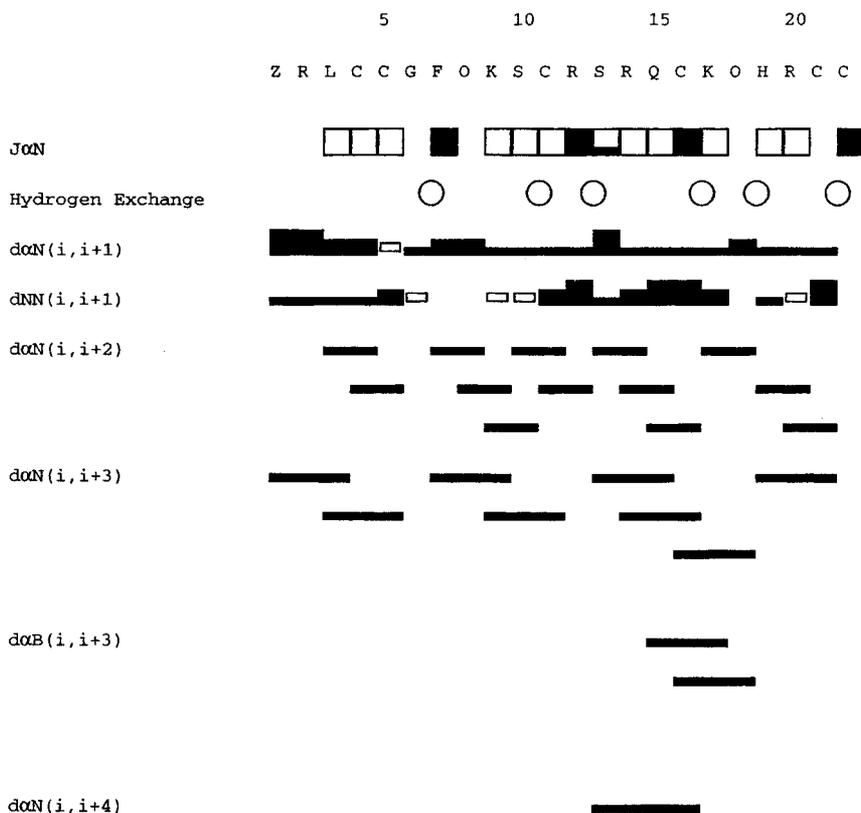
FIG. 6. **Local and medium range NOE, $^3J_{\text{NH-Hα}}$ coupling constant, and slow exchange data for PIIIA (pH 3, 280 K, 100% D$_2$O).** *Open circles*, NH protons that are present 2 h after the addition of D$_2$O. *Open squares*, $^3J_{\text{NH-Hα}} \leq 6$ Hz; *filled squares*, $^3J_{\text{NH-Hα}} \geq 8.5$ Hz; *partially filled squares*, 6 Hz $< {}^3J_{\text{NH-Hα}} < 8$ Hz. For NOE data, the *height* of *bars* indicates the strength of NOE. *Open bars* indicate peak overlap. Sequential NOEs involving Hδ$_i$-Hα$_{i-1}$ and Hδ$_i$-HN$_{i+1}$ distances, where $i$ = Hyp are represented in the dαN($i$, $i + 1$) and dNN($i$, $i + 1$) sections, respectively.

vides an additional means of checking and comparing NMR-derived structures, beyond a comparison of r.m.s. deviation values alone.

DISCUSSION

The present study confirms that μ-conotoxins PIIIA and PIIIA-(2–22) are potent blockers of neuronal VSSCs. It has been previously shown in radioligand binding studies that PIIIA and GIIIA discriminate among subtypes of the TTX-sensitive VSSC found in rat brain (26). This discrimination now extends to PIIIA-(2–22) and GIIIB in rat brain and to all μ-conotoxins except GIIIA in human brain. These differences in potency and extent of inhibition of rat and human brain VSSCs arise from relatively small sequence differences, with positions 14 and 18 influencing neuronal activity among the muscle-selective μ-conotoxins. Despite differential effects on neuronal TTX-S sodium channels in brain, GIIIA, GIIIB, and GIIIC have similar potency at skeletal muscle VSSCs. In the peripheral nervous system, PIIIA-(2–22) and PIIIA inhibit TTX-S VSSCs

without significantly affecting the TTX-R sodium current. Since μ-conotoxins have been shown to bind higher in the pore of Nav1.4 than TTX (53), it would appear that in addition to residue differences deep within the pore of the VSSC that render the channel TTX-R (54), additional changes occur further out in the pore to render TTX-R VSSCs insensitive to block by μ-conotoxins.

PIIIA and its analogue PIIIA-(2–22) are the first μ-conotoxins shown to distinguish between transient and persistent TTX-sensitive subtypes. Selective inhibition of persistent over transient VSSCs may control seizures, where the accompanying slow persistent sodium currents might be blocked without affecting the transient action potentials (7). It has been postulated that the persistent sodium channels are the same as those that generate transient sodium currents and that a small fraction of these channels enter a noninactivating mode to generate the persistent sodium current (55, 56). This type of persistent current has been observed in cell lines transfected

TABLE III
*Geometric and energetic statistics for the 20 structures of
μ-conotoxin PIIIA*

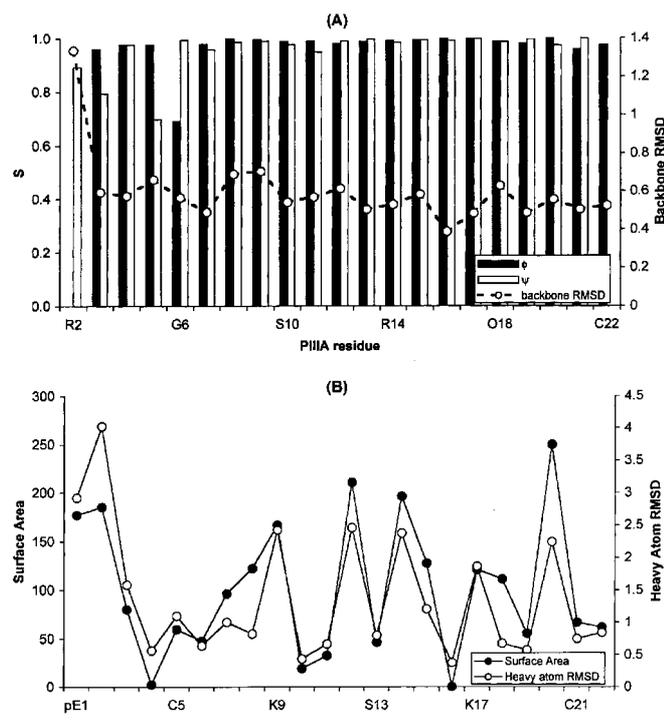| Parameter | Value |
|---|---|
| Mean r.m.s. deviations from experimental restraints | |
| NOE (Å) | $0.009 \pm 0.002$ |
| Dihedral (degrees) | $0.21 \pm 0.10$ |
| Mean r.m.s. deviation from idealized covalent geometry | |
| Bonds (Å) | $0.0079 \pm 0.0004$ |
| Angles (degrees) | $2.14 \pm 0.06$ |
| Impropers (degrees) | $0.19 \pm 0.02$ |
| Energies (kcal mol$^{-1}$) | |
| $E_{NOE}$ | $0.92 \pm 0.37$ |
| $E_{edih}$ | $0.05 \pm 0.04$ |
| $E_{L-J}$ | $-92.9 \pm 3.4$ |
| $E_{bond} + E_{angle} + E_{improper}$ | $47.3 \pm 3.1$ |
| Restraint violations | |
| Mean NOE violation (Å) | 0.029 |
| Maximum NOE violation (Å) | 0.17 |
| Mean dihedral angle violation (degrees) | 0.94 |
| Maximum angle violation (degrees) | 2.45 |



FIG. 7. *A*, backbone angular order parameters for the $\phi$ and $\psi$ dihedral angles and average backbone r.m.s. deviations *versus* PIIIA residue number. *B*, heavy atom r.m.s. deviations and the percentage of surface exposure (Å$^2$) *versus* PIIIA residue number.



FIG. 8. **Structure of PIIIA.** *A*, superimposition of the 20 lowest energy structures over the backbone region (residues 2–22). *B*, 180$_y$° rotation of the structures shown in *A* with the side chains of Ser[13] (*pink*), Arg[14] (*blue*), Gln[15] (*purple*), and Cys residues (*orange*) indicated. A comparison is shown of the positions of surface residues in PIIIA (*C*) and their counterparts in GIIIA (*D*). Note that the same surface-exposed residues are found in PIIIA and GIIIA and are all considered important for the potency of GIIIA to μ1 VSSCs (Nav1.4). *E* and *F*, comparison of core residues in PIIIA and GIIIA, respectively. Core residues differ between these two peptides and thus may contribute to selectivity differences at muscle and neuronal sodium channels. Side chains shown are Leu/Thr (*yellow*), Hyp/Ser (*pink*), Arg/Lys (*dark blue*), His (*light blue*), Gln (*purple*), Phe (*brown*), and Asp (*red*).

with cDNA for Na$_v$1.6 (11), Nav1.3 (13), or Nav1.2 (57). The persistent Na$^+$ current is also thought to play an important role in pacemaking currents and setting rythmicity in central neurons (58). During hypoxia or in the presence of free radicals (oxidative stress), these channels become more active (15, 17, 35) and could thus serve as a prominent pathway for Na$^+$ influx, triggering a cascade of damaging events that eventually cause cell damage and cell death (59). Hence, specific inhibitors of persistent Na$^+$ current may have neuroprotective effects. TTX, lidocaine, and quinidine can also inhibit persistent Na$^+$ channels without blocking transient Na$^+$ channels (14, 15). The μ-conotoxins extend the list of blockers able to discriminate between persistent and transient sodium currents.

Insights into the structure of the outer vestibule of the Nav1.4 channel have been obtained using the three-dimensional structure GIIIA and GIIIB as molecular calipers (21–23).
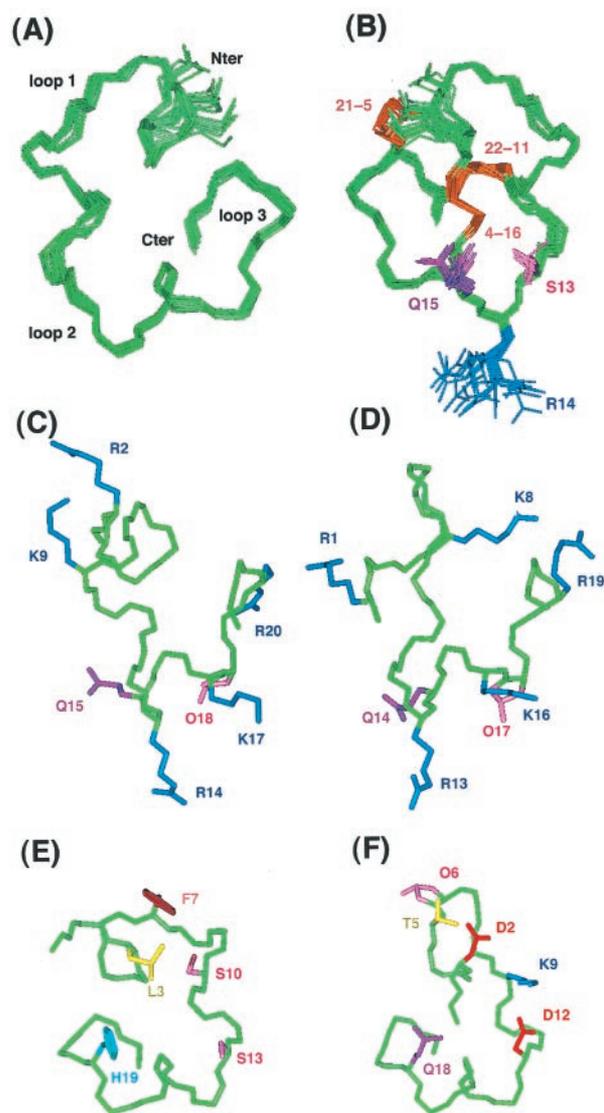
The fact that PIIIA is also able to block Nav1.4 indicates that many of the structural features found in GIIIA and GIIIB might also be conserved in PIIIA. However, additional structural differences must also exist to account for the high affinity of PIIIA and the structurally equivalent PIIIA-(2–22) at both neuronal and muscle forms of TTX-sensitive VSSCs. The three-dimensional structures of PIIIA are compared with those of GIIIA in Fig. 8, *C–F*. Although the positions of the C-terminal regions overlap and the positions of the functionally important Arg[14] (Arg[13] in GIIIA and GIIIB) are exposed in a similar manner, further comparison indicates marked differences in the orientation of the N-terminal region to the end of loop 1 at Cys 11. In GIIIB, this loop was described as forming a distorted β-hairpin that was suggested to exist also in GIIIA (20). This structural feature is not present in the major conformation of

PIIIA, where instead a series of loops exist. The structural difference between the major and minor forms arises from a difference at Hyp[8] (Hyp[7] in GIIIA), which adopts a predominately *trans* conformation in PIIIA but a *cis* conformation in GIIIA and GIIIB (19, 20). Importantly, residues including Lys[8]/Lys[9] and Arg[1]/Arg[2], which have been shown in GIIIA to be of moderate importance to binding, are placed in an entirely different position in the major conformation of PIIIA (Fig. 8, *C* and *D*). However, the effects of the *cis/trans* isomerization on the C-terminal region of PIIIA are minimal, with the conformation of the putatively important binding residues Arg[14], Arg[20], and Lys[17] not being significantly different from their GIIIA counterparts. The structural difference between the major forms of PIIIA, GIIIA, and GIIIB are unexpected, given that these peptides share the same disulfide connectivity and loop sizes and have considerable sequence homology. In contrast, the minor conformation of PIIIA, like GIIIA and GIIIB, arises from the *cis* form of Hyp[8]/Hyp[7], indicating that it adopts a three-dimensional structure more closely resembling GIIIA and GIIIB.

Comparison of the major conformation of PIIIA to a model of the minor conformation of PIIIA derived from the three-dimensional structure of GIIIA (Fig. 9) reveals that the positions of several side chains differ markedly between the two forms. Apart from the aforementioned structural differences at Arg[2] and Lys[9], the hydrophobic residues Leu[3] and Phe[7] are exposed to the solvent in the *cis* form yet hug the surface in the *trans* form, providing a different surface profile. In addition, the side chain of Cys[4] lies above the plane of the His[19] ring in the *trans* conformation (accounting for the ring current effects mentioned previously) but lies away from His[19] in the *cis* form, despite the fact that the position of His[19] is unchanged in either conformation. Thus, a simple *cis/trans* isomerization not only affects the surface of this peptide but somewhat surprisingly also alters the shape of part of the cysteine framework.

Conformational flexibility was proposed as a possible reason for the broadness of resonances associated with residues in the loop 2 of GIIIB (20). The present study shows that there are differing relative proportions and different rates of interconversion between the *cis/trans* forms. In GIIIA and GIIIB, it is apparent that the *cis* form predominates, with the *trans* form being masked by broadening associated with intermediate exchange occurring on the NMR time scale. In PIIIA, the *trans* form predominates, but the minor form is detectable because the two forms are in slow exchange. It is possible that the bulky Phe residue adjacent to Hyp[8] in PIIIA acts to slow the rate of Hyp isomerization. Two questions arise from the conformational heterogeneity found in PIIIA. First, which of the possible μ-conotoxin conformations binds to the VSSC? Second, what role is played by these conformational differences in determining VSSC selectivity among μ-conotoxins? Given that the broadened lines observed in GIIIA and GIIIB are indicative of alternative conformations, it is possible that a minor conformation of these muscle-selective μ-conotoxins binds to the VSSCs. If this is indeed correct, it could impact on studies investigating the structure of the outer vestibule of the VSSC using the currently available structures of μ-conotoxins.

Apart from Arg[14], which has been shown to be important for the activity of PIIIA, it is not known which other residues in this peptide are involved in VSSC binding. An examination of the three-dimensional structures and the surface profile (Fig. 7*B*) of PIIIA reveals residues that are on the surface (Fig. 8*C*) and are hence potentially available for interactions with the sodium channel. Along with Arg[14], these include Lys[17], Hyp[18], and Arg[20], which parallel residues Lys[16], Hyp[17], and Arg[19] in GIIIA (Fig. 8*D*), thus defining a common pharmacophore, as
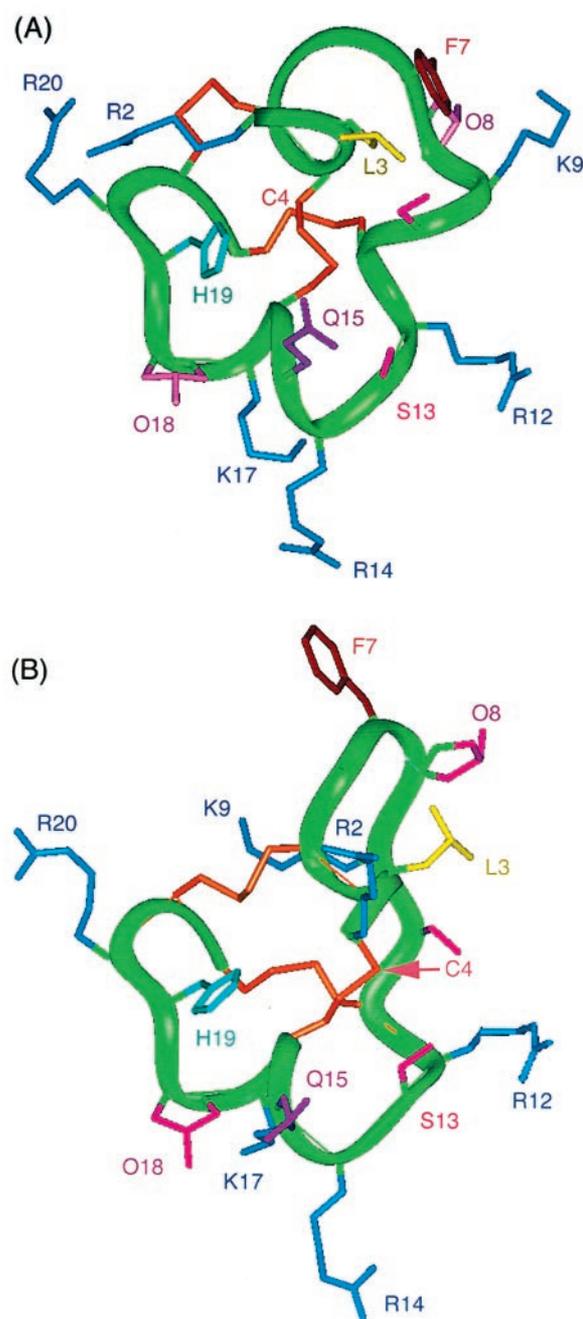


FIG. 9. **Comparison of the major conformation of PIIIA (*A*) with a modeled structure of its minor conformation (*B*).** The minor conformation was modeled from the structure of the major conformation of GIIIB (20). Structures are superimposed for Arg[12] to Cys[22]. Side chains are labeled as in Fig. 8.

previously suggested (26). Note that Ser[13] is buried, consistent with it playing a structural role that ensures the exposure of Arg[14]. In GIIIA, the residue Asp[12], which corresponds to Ser[13] in PIIIA, may also play a structural role. The other exposed residues, Lys[9] and Arg[2], have structural counterparts in GIIIA (Lys[8] and Arg[1]) but adopt quite different positions in the predominant conformations of these two peptides.

It is interesting that the residues that differ between PIIIA and GIIIA cluster on one face of the peptide, perhaps forming a functionally significant pocket or cavity (Fig. 8, *E* and *F*). It is possible that one or more of these mostly hydrophobic and polar residues contribute to binding to the neuronal VSSCs and thus confer broader specificity to PIIIA (and PIIIA-(2–22)). Thus, core residues and the positioning of exposed residues that differ

between the μ-conotoxins may contribute to selectivity differences of μ-conotoxins at VSSCs. The results from this study show that the μ-conotoxin framework is less conformationally conserved than previously suspected and illustrate the need for careful analysis of the range of structures this class of conotoxins can access. The structure of PIIIA described here provides a new molecular caliper for neuronal and muscle VSSCs.

## REFERENCES

1. Catterall, W. A. (2000) *Neuron* **26,** 13–25
2. Goldin, A. L. Barchi, R. L, Caldwell, J. H., Hofmann, F., Howe, J. R., Hunter, J. C., Kallen, R. G., Mandel, G., Meisler, M. H., Netter, Y. B., Noda, M., Tamkun, M. M., Waxman, S. G., Wood, J. N., and Catterall, W. A. (2000) *Neuron* **28,** 365–368
3. Akopian, A. N., Souslova, V., England, S., Okuse, K., Ogata, N., Ure, J., Smith, A., Kerr, B. J., McMahon, S. B., Boyce, S., Hill, R., Stanfa, L. C., Dickenson, A. H., and Wood, J. N. (1999) *Nat. Neurosci.* **6,** 541–548
4. Eglen, R. M., Hunter, J. C., and Dray, A. (1999) *Trends Pharmacol. Sci.* **20,** 337–342
5. Porreca, F., Lai, J., Bian, D., Wegert, S., Ossipov, M. H., Eglen, R. M., Kassotakis, L., Novakovic, S., Rabert, D. K., Sangameswaran, L., and Hunter, J. C. (1999) *Proc. Natl. Acad. Sci. U. S. A.* **96,** 7640–7644
6. Coward, K., Plumpton, C., Facer, P., Birch, R., Carlstedt, T., Tate, S., Bountra, C., and Anand, P. (2000) *Pain* **85,** 41–50
7. Taylor, C. P., and Meldrum, B. S. (1995) *Trends Pharmacol. Sci.* **16,** 309–316
8. Carter, A. J. (1998) *Amino Acids* **14,** 159–169
9. Ragsdale, D. S., and Avoli, M. (1998) *Brain Res. Brain Res. Rev.* **26,** 16–28
10. Rho, J. M., and Sankar, R. (1999) *Epilepsia* **40,** 1471–1483
11. Smith, M. R., Smith, R. D., Plummer, N. W., Meisler, M. H., and Goldin, A. L. (1998) *J. Neurosci.* **18,** 6093–6102
12. Bevan, M. D., and Wilson, C. J. (1999) *J. Neurosci.* **19,** 7617–7628
13. Moorman, J. R., Kirsch, G. E., Vandongen, A. M., Joho, R. H., and Brown, A. M. (1990) *Neuron* **4,** 243–252
14. Ju, Y., Saint, D. A., and Gage, P. W. (1992) *Br. J. Pharmacol.* **107,** 311–316
15. Hammarström, A. K., and Gage, P. W. (1998) *J. Physiol.* **510,** 735–741
16. Hammarström, A. K., and Gage, P. W. (2000) *J. Physiol.* **529,** 107–118
17. Hammarström, A. K., and Gage, P. W. (1999) *J. Physiol.* **520,** 451–461
18. Whitaker, W. R., Faull, R. L. M., Waldvogel, H. J., Plumpton, C. J., Emson, P. C., and Clare, J. J. (2001) *Mol. Brain Res.* **88,** 37–53
19. Lancelin, J-M., Kohda, D., Tate, S., Yanagawa, Y., Abe, T., Satake, M., and Inagaki, F. (1991) *Biochemistry* **30,** 6908–6916
20. Hill, J. M., Alewood, P. F., and Craik, D. J. (1996) *Biochemistry* **35,** 8824–8835
21. Chahine, M., Chen, L-Q., Fotouhi, N., Walsky, R., Fry, D., Santarelli, V., Horn, R., and Kallen, R. G. (1995) *Receptors Channels* **3,** 161–174
22. Chang, N., French, R. J., Lipkind, G. M., Fozzard, H. A., and Dudley, S., Jr. (1998) *Biochemistry* **37,** 4407–4419
23. Li, R. A., Ennis, I. L., Velez, P., Tomaselli, G. F., and Marban, E. (2000) *J. Biol. Chem.* **275,** 27551–27558
24. Lipkind, G. M., and Fozzard, H. A. (2000) *Biochemistry* **39,** 8161–8170
25. Li, R. A., Ennis, I. I., French, R. J., Dudley, S. C., Tomaselli, G. F., and Marban, E. (2001) *J. Biol. Chem.* **276,** 11072–11077
26. Shon, K-J., Olivera, B. M., Watkins, M., Jacobsen, R. B., Gray, W. R., Floresca, C. Z., Cruz, L. J., Hillyard, D. R., Brink, A., Terlau, H., and Yoshikami, D. (1998) *J. Neurosci.* **18,** 4473–4481
27. Safo, P., Rosenbaum, T., Shcherbatko, A., Choi, D. Y., Han, E., Toledo-Aral, J. J., Olivera, B. M., Brehm, P., and Mandel, G. (2000) *J. Neurosci.* **20,** 76–80
28. Schnölzer, M., Alewood, P. F., Jones, A., Alewood D., and Kent, S. B. H. (1992) *Int. J. Pept. Protein Res.* **40,** 180–193
29. Nielsen, K. J., Adams, D., Thomas, L., Bond, T. J., Alewood, P. F., Craik D. J., and Lewis, R. J. (1999) *J. Mol. Biol.* **289,** 1405–1421
30. Maddison, J. E., Dodd, P. R., Johnston, G. A. R., and Farrell, G. C. (1987) *Gastroenterology*, **93,** 1062–1068
31. Yanagawa, Y., Abe, T., Satake, M., Odani, S., Suzuki, J., and Ishikawa, K. (1988) *Biochemistry* **27,** 6256–6262
32. Jeglitsch, G., Rein, K., Baden, D. G., and Adams, D. J. (1998) *J. Pharmacol. Exp. Ther.* **284,** 516–525
33. Nicholson, G. M., Walsh, R., Little, M. J., and Tyler, M. I. (1998) *Pflugers Arch.* **436,** 117–126
34. Elliott, A. A., and Elliott, J. R. (1993) *J. Physiol.* **463,** 39–56
35. Ju, Y. K., Saint, D. A., and Gage, P. W. (1996) *J. Physiol.* (*Lond.*) **497,** 337–347
36. Jeener, J., Meier, B. H., Bachmann, P., and Ernst, R. R. (1979) *J. Chem. Phys.* **71,** 4546–4553
37. Kumar, A., Ernst, R. R., and Wüthrich, K. (1980) *Biochem. Biophys. Res. Commun.* **95,** 1–6
38. Bax, A., and Davis, D. G. (1985) *J. Magn. Reson.* **65,** 355–360
39. Rance, M., Sørenson, O. W., Bodenhausen, G., Wagner, G., Ernst, R. R., and Wüthrich, K. (1983) *Biochem. Biophys. Res. Commun.* **177,** 479–485
40. Greisinger, C., Sorenson, O. W., and Ernst, R. R. (1987) *J. Magn. Reson.* **75,** 474–492
41. Piotto, M., Saudek, V., and Sklenár, V. (1992) *J. Biolmol. NMR* **2,** 661–665
42. Wishart, D. S., Bigam, C. G., Yao, J., Abildgaard, F., Dyason, H. J., Oldfield, E., Markley, J. L., and Sykes, B. D. (1995) *J. Biomol. NMR* **5,** 67–81
43. Wüthrich, K., Billeter, M., and Braun, W. (1983) *J. Mol. Biol.* **169,** 949–961
44. Pardi, A., Billeter, M., and Wüthrich, K. (1984) *J. Mol. Biol.* **180,** 741–751
45. Wagner, G., Braun, W., Havel, T. F., Schaumann, T., Go, N., and Wüthrich, K. (1987) *J. Mol. Biol.* **196,** 611–639
46. Brünger, A. T. (1992) *X-PLOR: A System for X-ray Crystallography and NMR*, Version 3.1, Yale University, New Haven, CT
47. Brooks, B., Brucoli, R., Olafson, B. O., States, D., Swaminathan, S., and Karplus, M. (1983) *J. Comput. Chem.* **4,** 187–217
48. Koradi, R., Billeter M., and Wuthrich, K. (1996) *J. Mol. Graph.* **51,** 29–32
49. Laskowski, R. A., MacArthur, M. W., and Thornton, J. M. (1998) *Curr. Opin. Struct. Biol.* **8,** 631–639
50. French, C. R., and Gage, P. W. (1985) *Neurosci. Lett.* **56,** 289–293
51. French, C. R., Sah, P., Buckett, K. J., and Gage, P. W. (1990) *J. Gen. Physiol.* **95,** 1139–1157
52. Wüthrich, K. (1986) *NMR of Proteins and Nucleic Acids*, Wiley-Interscience, New York
53. Dudley, S. C., Jr., Todt, H., Lipkind, G., and Fozzard, H. A. (1995) *Biophys. J.* **69,** 1657–1665
54. Satin, J., Kyle, J. W., Chen, M., Bell, P., Cribbs, L. L., Fozzard, H. A., and Rogart, R. B. (1992) *Science* **256,** 1202–1205
55. Alzheimer, C., Schwindt, P. C., and Crill, W. E. (1993) *J. Neurosci.* **13,** 660–673
56. Crill, W. E. (1996) *Annu. Rev. Physiol.* **58,** 349–362
57. Numann, R., Catterall, W. A., and Scheuer, T. (1991) *Science* **254,** 115–118
58. Taylor, C. P. (1993) *Trends Neurosci.* **16,** 455–460
59. Taylor, C. P., and Narasimhan, L. S. (1997) *Adv. Pharmacol.* **39,** 47–98
60. Cruz, L. J., Gray, W. R., Olivera, B. M., Zeikus, R. D., Kerr, L., Yoshikami, D., and Moczydlowski, E. (1985) *J. Biol. Chem.* **260,** 9280–9288